

Article

## Hot Deformation Mechanisms in AZ31 Magnesium Alloy Extruded at Different Temperatures: Impact of Texture

Kamineni Pitcheswara Rao <sup>1,\*</sup>, Yellapregada Venkata Rama Krishna Prasad <sup>2</sup>,  
Joanna Dzwonczyk <sup>3</sup>, Norbert Hort <sup>4</sup> and Karl Ulrich Kainer <sup>4</sup>

<sup>1</sup> Department of Mechanical and Biomedical Engineering, City University of Hong Kong, Tat Chee Avenue, Kowloon, Hong Kong SAR, China

<sup>2</sup> Processingmaps.com, No. 2/B, Hospital Extension, Vinayak Nagar, Bangalore 560075, India; E-Mail: prasad\_yvrk@hotmail.com

<sup>3</sup> Lightweight Metallic Materials, SKF Engineering & Research Centre, Utrecht Area, Netherlands; E-Mail: j.s.dzwonczyk@tudelft.nl

<sup>4</sup> Magnesium Innovation Centre, Helmholtz Zentrum Geesthacht, Max-Planck-Straße 1, Geesthacht 21502, Germany; E-Mails: norbert.hort@hzg.de (N.H.); karl.kainer@hzg.de (K.U.K.)

\* Author to whom correspondence should be addressed; E-Mail: mekprao@cityu.edu.hk; Tel.: +852-3442-8409; Fax: +852-3442-0172.

Received: 25 June 2012; in revised form: 27 July 2012 / Accepted: 6 August 2012 /

Published: 23 August 2012

---

**Abstract:** The hot deformation characteristics of AZ31 magnesium alloy rod extruded at temperatures of 300 °C, 350 °C and 450 °C have been studied in compression. The extruded material had a fiber texture with  $\langle 10\bar{1}0 \rangle$  parallel to the extrusion axis. When extruded at 450 °C, the texture was less intense and the  $\langle 10\bar{1}0 \rangle$  direction moved away from the extrusion axis. The processing maps for the material extruded at 300 °C and 350 °C are qualitatively similar to the material with near-random texture (cast-homogenized) and exhibited three dynamic recrystallization (DRX) domains. In domains #1 and #2, prismatic slip is the dominant process and DRX is controlled by lattice self-diffusion and grain boundary self-diffusion, respectively. In domain #3, pyramidal slip occurs extensively and DRX is controlled by cross-slip on pyramidal slip systems. The material extruded at 450 °C exhibited two domains similar to #1 and #2 above, which moved to higher temperatures, but domain #3 is absent. The results are interpreted in terms of the changes in  $\langle 10\bar{1}0 \rangle$  fiber texture with extrusion temperature. Highly intense  $\langle 10\bar{1}0 \rangle$  texture, as in the rod extruded at 350 °C, will enhance the occurrence of prismatic slip in domains #1 and #2 and promotes pyramidal slip at temperatures >450 °C (domain #3).

**Keywords:** AZ31 magnesium alloy; extrusion temperature; fiber texture; processing maps; kinetic analysis

---

## 1. Introduction

In recent years magnesium alloys are being given increasing attention as light-weight high specific stiffness materials for use as structural parts in aerospace, automobile and computer hardware applications [1]. Among the wrought alloys, Mg-3Al-1Zn (AZ31) is being investigated in detail as regards processing–microstructure–property correlations [2–11]. Primary working of magnesium materials is done by the extrusion process [12–15], which is generally conducted at higher temperatures to take advantage of enhanced workability caused by the participation of non-basal slip. AZ31 is commercially extruded at about 300 °C to obtain a fine grained structure. The product, however, also develops a crystallographic texture which, in the case of a rod, is a fiber texture with  $\langle 10\bar{1}0 \rangle$  parallel to the extrusion direction (ED) [2,6]. An increase in the extrusion temperature increases the grain size [9] but its effect on the texture is not clearly known. The initial microstructure has a strong influence on the hot working behavior of AZ31 alloy [2] which is through the effect of the initial texture [16] on the dynamic recrystallization (DRX) process. Wu and Liu [17] reported that even large grained AZ31 exhibits superplastic deformation when deformed at 500 °C due to the occurrence of DRX in the initial stages of deformation resulting in a stable fine grain size. Alternately, Tan and Tan [18] reported a two stage method of first refining the grain size by a lower temperature (250 °C) deformation and then by deforming at much higher temperatures (400 °C or 450 °C). In both the above methods, not only does the grain size change but also the texture, both of which influence the response to hot deformation [10]. The aim of the present investigation is to evaluate the influence of extrusion temperature on the hot working characteristics of AZ31 extruded product through its effect primarily on the texture developed in the starting material. With a view to bring out the effect of texture, the results obtained on the extruded alloy have been compared with those obtained on cast-homogenized AZ31 [19] with a near-random texture.

The hot deformation behavior is explored using the methods of kinetic analysis as well as processing maps. The former one is based on the standard kinetic rate equation relating the flow stress ( $\sigma$ ) to strain rate ( $\dot{\epsilon}$ ) and temperature ( $T$ ), given by [20]:

$$\dot{\epsilon} = A\sigma^n \exp[-Q/RT] \quad (1)$$

where  $A$  = constant,  $n$  = stress exponent,  $Q$  = activation energy, and  $R$  = gas constant. The rate-controlling mechanisms are identified on the basis of the activation parameters  $n$  and  $Q$ . The kinetics of hot working in Mg-Al-Zn alloys has been reviewed recently [21] and the apparent activation energy values estimated by different investigators [22–26] have shown some variations and are generally higher than that for lattice self-diffusion in magnesium.

The technique of processing maps is based on the dynamic materials model, the principles of which are described earlier [27–29]. Briefly, the work piece undergoing hot deformation is considered to be a dissipater of power and the strain rate sensitivity ( $m$ ) of flow stress is the factor that partitions power between deformation heat and microstructural changes. The efficiency of power dissipation ( $\eta$ )

occurring through microstructural changes during deformation is derived by comparing the non-linear power dissipation occurring instantaneously in the work-piece with that of a linear dissipater for which the  $m$  value is unity, and is given by:

$$\eta = 2m/(m + 1) \quad (2)$$

The variation of efficiency of power dissipation with temperature and strain rate represents a *power dissipation map* which is generally viewed as an iso-efficiency contour map. Further, the extremum principles of irreversible thermodynamics as applied to continuum mechanics of large plastic flow [30] are explored to define a criterion for the onset of flow instability given by the equation for the instability parameter  $\xi(\dot{\epsilon})$ :

$$\xi(\dot{\epsilon}) = \frac{\partial \ln[m/(m+1)]}{\partial \ln \dot{\epsilon}} + m \leq 0 \quad (3)$$

The variation of the instability parameter as a function of temperature and strain rate represents an *instability map* which delineates regimes of instability where  $\xi$  is negative. A superimposition of the *instability map* on the power dissipation map gives a *processing map* which reveals *domains* (efficiency contours converging towards a peak efficiency) where individual microstructural processes occur and the limiting conditions for the *regimes* (bounded by a contour for  $\xi = 0$ ) of flow instability. Processing maps help in identifying temperature–strain rate windows or domains for hot working where the intrinsic workability of the material is maximum (e.g., dynamic recrystallization (DRX) or superplasticity) and also in avoiding the *regimes* of flow instabilities (e.g., adiabatic shear bands or flow localization). The kinetic rate equation is obeyed by the data within the *domains* since they are “deterministic” and the data in the change-over regions (termed *bifurcations*) show deviations [31]. The processing-map technique has been highly successful in evaluating the hot deformation mechanisms in a wide range of Mg and its alloys [32–41] including DRX and flow instabilities.

## 2. Experimental Section

The AZ31 magnesium used in this investigation was a commercial AZ31B alloy with the composition (wt.%) of Al—3.1%, Zn—0.98%, Mn—0.2%. Cylindrical rods were direct-extruded isothermally at billet temperatures of 300 °C and 350 °C using a ram speed of 6.7 mm/s and extrusion ratio of 23:1 while the extrusion at 450 °C was done at a ram speed of 3.2 mm/s and an extrusion ratio of 17:1. Cylindrical specimens of 10 mm diameter and 15 mm height were machined from the extruded rods with their compression axis parallel to ED. For inserting a thermocouple to measure the specimen temperature as well as the adiabatic temperature rise during deformation, the specimens are provided with a 1 mm diameter hole machined at mid-height to reach the center of the specimen.

The specimens from the rods extruded at 300 °C and 350 °C were tested in uniaxial compression in a constant true strain rate range 0.001–100 s<sup>-1</sup> and temperature range 300–550 °C. The specimens from the rod extruded at 450 °C were tested in compression in the temperature range 250–550 °C and strain rate range 0.0003–10 s<sup>-1</sup>. Details of the test set-up and procedure are described in earlier publication [42]. Constant true strain rates during the tests were achieved using an exponential decay of actuator speed in the servo-hydraulic machine. Graphite powder mixed with grease was used as the lubricant in all the experiments. The specimens were deformed up to a true strain of about 0.7 and

quenched in water. The load-stroke data were converted into true stress-true strain curves using standard equations. The flow stress values were corrected for the adiabatic temperature rise using the temperature measured during testing. Processing maps were developed using the procedures described earlier [28] and with the flow stress data at different temperatures, strain rates and strains obtained from the above experiments as input. For metallographic examination, the deformed specimens were sectioned in the center parallel to the compression axis and the cut surface was mounted, polished and etched with an aqueous solution containing 10% picric acid. The average grain diameter was measured using linear intercept method. The texture in the starting material was evaluated using a TEX-2 neutron diffractometer and represented as inverse pole figures [43] which are useful in the case of extruded rods since only a single axis has to be specified. The inverse pole figures consist of a single triangle of the stereographic projection within which the frequency of a particular crystallographic direction coinciding with the specimen axis is plotted.

### 3. Results and Analysis

#### 3.1. Initial Microstructure and Texture

The microstructures of the cast-homogenized AZ31 alloy and the rods extruded at 300, 350 and 450 °C are shown in Figure 1(a–d). The cast material had a large grain size while the rods extruded at 300 °C, 350 °C and 450 °C exhibited finer equiaxed grains with average grain diameters of 12, 16 and 9 μm, respectively. Thus the grain sizes of the extrusions are in a similar range. The cast-homogenized alloy had near-random texture and may be used as a reference material for evaluating the behavior of extruded rods. The inverse pole figures obtained on the three starting extrusion rods are given in Figure 2(a–c), which show the results obtained on the sections normal to ED. The figures indicate that  $\langle 10\bar{1}0 \rangle$  is parallel ED and the intensity of this texture is about 3.22, 3.76 and 2.5 times that of random for 300 °C, 350 °C and 450 °C extrusions respectively.

The development of texture during extrusion may be analyzed in terms of a simple flow model involving different slip systems. During extrusion of a randomly textured material at 300 °C or 350 °C, all the crystallites which are favorably oriented (45° with respect to ED) for basal + prismatic slip undergo plastic deformation. During flow, the basal planes rotate and align themselves parallel to ED, and the associated prismatic slip on one set of planes makes ED align with  $\langle 10\bar{1}0 \rangle$ . However, when the extrusion temperature is increased to 450 °C, pyramidal slip gets activated along with considerable cross-slip which will reduce the  $\langle 10\bar{1}0 \rangle$  fiber texture and move the  $\langle 10\bar{1}0 \rangle$  pole away from the extrusion direction. Thus, extrusion at temperatures higher than 450 °C where pyramidal slip systems dominate the flow and a concomitant cross-slip will reduce the development of textures in AZ31.

**Figure 1.** Microstructures obtained on AZ31: (a) cast-homogenized condition; extruded at: (b) 300 °C; (c) 350 °C; and (d) 450 °C.

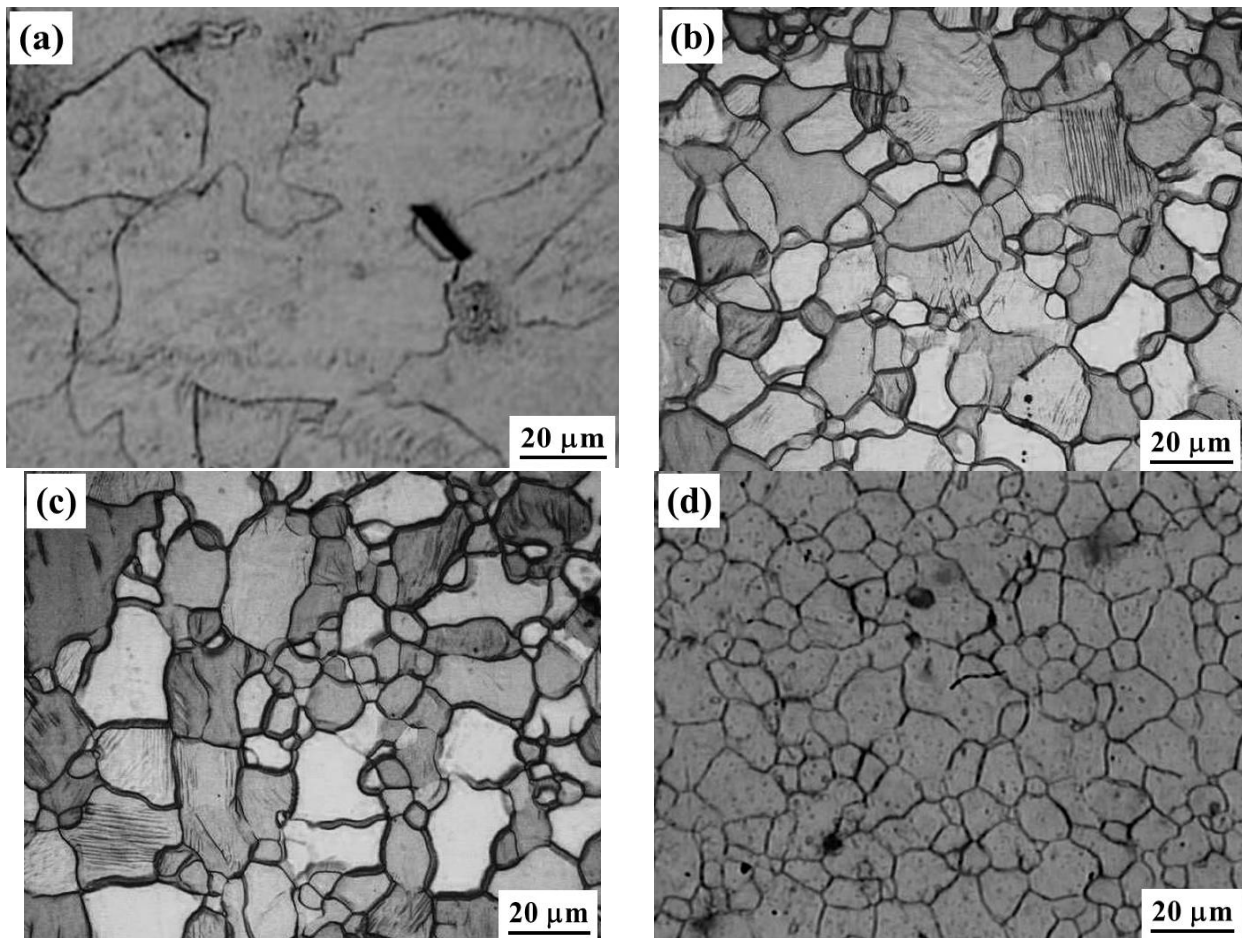


**Figure 2.** Inverse pole figures recorded on the plane perpendicular, and the mid-plane parallel to the extrusion direction of AZ31 rod extruded at: (a) 300 °C; (b) 350 °C; and (c) 450 °C.

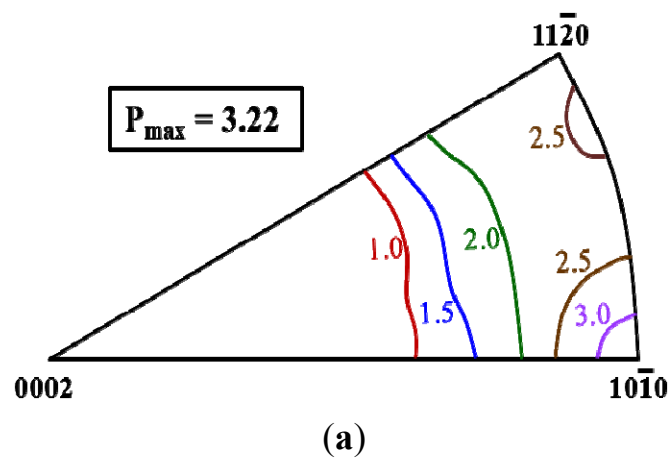
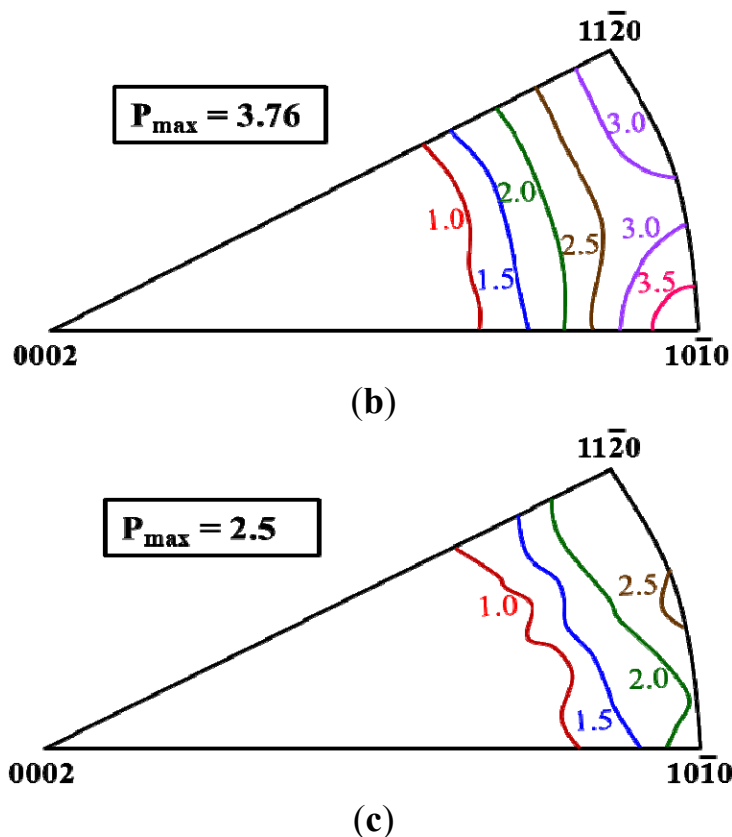


Figure 2. Cont.



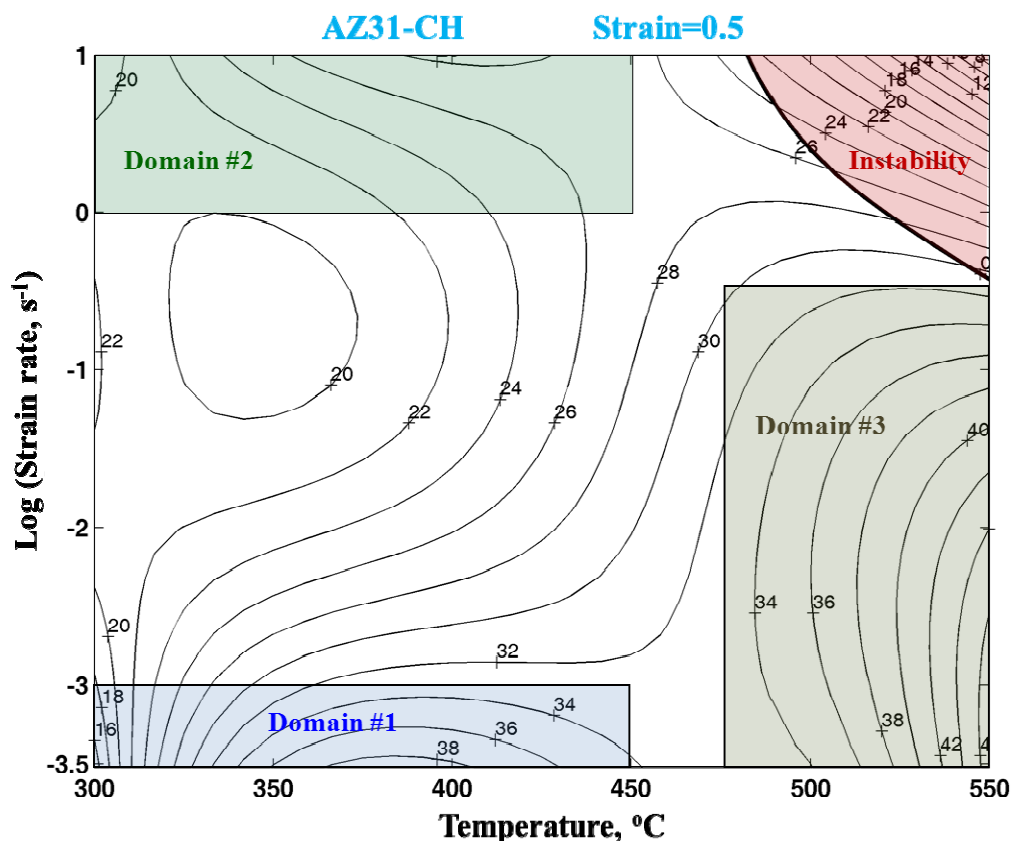
### 3.2. Cast-Homogenized AZ31 Alloy

The hot working behavior of cast-homogenized AZ31 alloy was characterized in detail in an earlier publication [19]. For the purpose of comparison, the processing map obtained on this material is shown in Figure 3, which exhibits three domains in the temperature and strain rate ranges as follows: (1) 300–450 °C/0.0003–0.001 s<sup>-1</sup> with a peak efficiency of 38% occurring at 375 °C/0.0003 s<sup>-1</sup>; (2) 300–450 °C/1–10 s<sup>-1</sup> with a peak efficiency of 28% occurring at 400 °C/10 s<sup>-1</sup>; and (3) 475–550 °C/0.0003–0.3 s<sup>-1</sup> with a peak efficiency of 46% occurring at 550 °C/0.001 s<sup>-1</sup>. In addition, a regime of flow instability occurs at temperatures higher than 475 °C and strain rates higher than about 0.3 s<sup>-1</sup>. Detailed microstructural analysis in the three domains above indicated that they represent DRX process [19].

It is well established that in magnesium materials, four different slip systems operate if their critical resolved shear stress (CRSS) is exceeded and these are: (1) basal slip  $\{0002\} \langle 11\bar{2}0 \rangle$ ; (2) prismatic slip  $\{10\bar{1}0\} \langle 11\bar{2}0 \rangle$ ; (3) first order pyramidal slip  $\{10\bar{1}1\} \langle 11\bar{2}0 \rangle$  and  $\{10\bar{1}2\} \langle 11\bar{2}0 \rangle$ ; and (4) second order pyramidal slip  $\{11\bar{2}2\} \langle 11\bar{2}3 \rangle$ . In polycrystalline magnesium, while basal slip is the easiest to occur, prismatic slip contributes significantly to plastic flow at temperatures higher than about 225 °C and pyramidal slip is dominant beyond about 450 °C. In the cast alloy which has a near-random texture, basal + prismatic slip occur in domains #1 and #2 of the map, while pyramidal slip particularly  $\{11\bar{2}2\} \langle 11\bar{2}3 \rangle$  is likely to contribute to plastic flow in domain #3. The recovery mechanism associated with basal + prismatic slip is the climb process since the stacking fault energy

on basal planes is low ( $60\text{--}78\text{ mJ/m}^2$ ) [44], while it is cross-slip at higher temperatures where pyramidal slip occurs since the stacking fault energy on pyramidal planes is high ( $173\text{ mJ/m}^2$ ) [45].

**Figure 3.** Processing map for AZ31 in cast-homogenized conditions (near-random texture) obtained at a strain of 0.5. The numbers against the contours represent efficiency of power dissipation in percent. The regime of flow instability is marked.



With a view to evaluate the rate-controlling mechanisms for DRX in the three domains identified in the map, kinetic analysis has been conducted using Equation (1). The Arrhenius plot showing the variation of flow stress normalized with shear modulus ( $\mu$ ) in the form of  $\ln(\sigma/\mu)$  vs.  $(1/T)$  is shown in Figure 4. It may be noted that the kinetic rate equation is obeyed only within each of the deterministic domains and deviations occur in the change-over regions. In domain #1, the apparent activation energy is  $131\text{ kJ/mol}$ , which is close to that for lattice self-diffusion in pure magnesium ( $135\text{ kJ/mol}$ ) [46]. In domain #2, the apparent activation energy is  $110\text{ kJ/mole}$  which is near that for grain boundary self-diffusion ( $92\text{ kJ/mol}$ ) [46]. In domain #3, the apparent activation energy is much higher ( $190\text{ kJ/mol}$ ) than that for self-diffusion and suggests cross-slip mechanism. The results on the domain characteristics and kinetic parameters are summarized in Table 1. Thus, in both domains #1 and #2 where basal + prismatic slip dominates, DRX is controlled by dislocation climb process which depends on lattice self-diffusion if the strain rates are slow (domain #1) and on faster grain boundary self-diffusion if the strain rates are high (domain #2). In the high temperature domain (domain #3), DRX is caused by second-order pyramidal slip and associated recovery by cross-slip which can easily occur since many slip planes are active in this system.

**Figure 4.** Arrhenius plot for calculating apparent activation energy in the three domains of processing map for cast-homogenized AZ31 magnesium alloy (near-random texture).

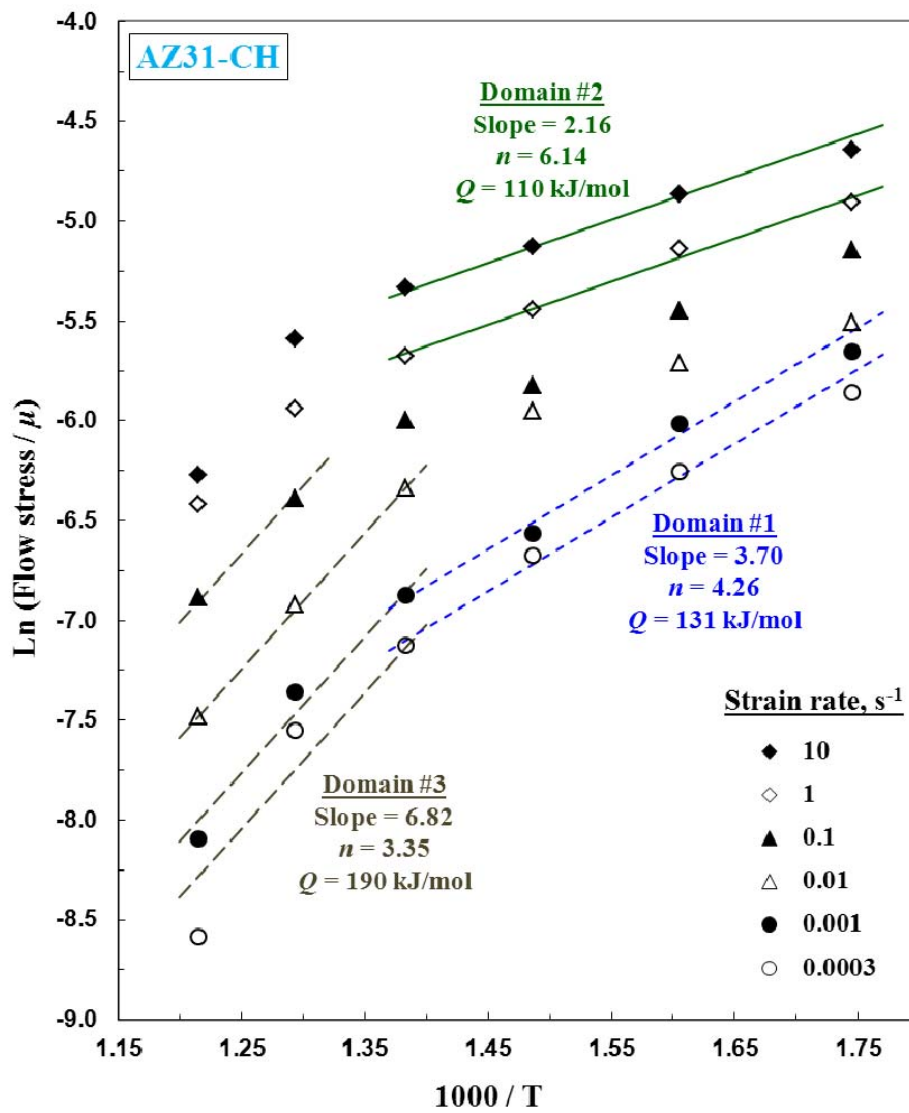


**Table 1.** Summary of results from processing maps and kinetic analysis of the temperature and strain rate dependence of flow stress in compression for AZ31 alloy in cast-homogenized conditions and after extruding at different temperatures.

| Material condition              | Domain    | Domain characteristics                    |  | Kinetic parameters |              | Suggested mechanism              |
|---------------------------------|-----------|---|--|--------------------|--------------|----------------------------------|
|                                 |           | $T$ & $\dot{\epsilon}$ range              | Peak $\eta$ at $T$ & $\dot{\epsilon}$  | $n$                | $Q$ , kJ/mol |                                  |
| C-H<br>(Near-random<br>Texture) | Domain #1 | 300–450 °C & 0.0003–0.001 s <sup>-1</sup> | 38% at 375 °C & 0.0003 s <sup>-1</sup> | 4.26               | 131          | DRX/Lattice Diffusion            |
|                                 | Domain #2 | 300–450 °C & 1–10 s <sup>-1</sup>         | 28% at 400 °C & 10 s <sup>-1</sup>     | 6.14               | 110          | DRX/Grain Boundary Diffusion     |
|                                 | Domain #3 | 475–550 °C & 0.0003–0.3 s <sup>-1</sup>   | 46% at 550 °C & 0.001 s <sup>-1</sup>  | 3.35               | 190          | DRX/Cross-slip                   |
| Extruded at<br>300 °C           | Domain #1 | 300–450 °C & 0.001–0.01 s <sup>-1</sup>   | 34% at 400 °C & 0.001 s <sup>-1</sup>  | 4.88               | 138          | DRX/Lattice Diffusion            |
|                                 | Domain #2 | 300–450 °C & 1–10 s <sup>-1</sup>         | 46% at 300 °C & 10 s <sup>-1</sup>     | 5.26               | 103          | DRX/Grain Boundary Diffusion     |
|                                 | Domain #3 | 450–550 °C & 0.001–0.1 s <sup>-1</sup>    | 48% at 550 °C & 0.001 s <sup>-1</sup>  | 3.85               | 184          | DRX/Cross-slip                   |
| Extruded at<br>350 °C           | Domain #1 | 300–450 °C & 0.001–0.01 s <sup>-1</sup>   | 56% at 375 °C & 0.001 s <sup>-1</sup>  | 5.33               | 133          | DRX/Lattice Diffusion            |
|                                 | Domain #2 | 300–450 °C & 1–10 s <sup>-1</sup>         | 42% at 350 °C & 10 s <sup>-1</sup>     | 5.60               | 105          | DRX/Grain Boundary Diffusion     |
|                                 | Domain #3 | 500–550 °C & 0.001–0.01 s <sup>-1</sup>   | 82% at 550 °C & 0.001 s <sup>-1</sup>  | 4.16               | 160          | DRX/Cross-slip (Superplasticity) |
| Extruded at<br>450 °C           | Domain #1 | 300–550 °C & 0.0003–0.003 s <sup>-1</sup> | 44% at 475 °C & 0.0003 s <sup>-1</sup> | 4.21               | 137          | DRX/Lattice Diffusion            |
|                                 | Domain #2 | 275–525 °C & 1–10 s <sup>-1</sup>         | 44% at 400 °C & 10 s <sup>-1</sup>     | 5.00               | 104          | DRX/Grain Boundary Diffusion     |
|                                 | Domain #3 |   | **** ABSENT ****                       |                    |              |                                  |

### 3.3. Hot Compression of AZ31 Extruded at 300 °C

The processing map obtained at a strain of 0.4 is shown in Figure 5 which is a typical representation under steady-state flow conditions. The map is qualitatively similar to that for cast-homogenized material (near-random texture) (Figure 3) in the sense that it also exhibits three similar domains. The temperature and strain rate ranges for these domains are as follows: (1) 300–450 °C/0.001–0.01 s<sup>-1</sup> with a peak efficiency of 34% occurring at 400 °C/0.001 s<sup>-1</sup>, (2) 300–450 °C/1–10 s<sup>-1</sup> with a peak efficiency of 46% occurring at 300 °C/10 s<sup>-1</sup>, (3) 450–550 °C/0.001–0.1 s<sup>-1</sup> with a peak efficiency of 48% occurring at 550 °C/0.001 s<sup>-1</sup>. When compared with the map for cast-homogenized material the peak efficiency values are marginally higher and the peak in domain #2 has moved to lower temperatures. The microstructures of specimens deformed at 400 °C/0.001 s<sup>-1</sup> (domain #1), 300 °C/10 s<sup>-1</sup> (domain #2) and 550 °C/0.001 s<sup>-1</sup> (domain #3) are shown in Figure 6(a–c), which represent DRX. The microstructures in domains #1 and #2 have some curved grain boundaries typical of DRX. However, in domain #3 the microstructure resembles a “diamond” configuration where a high population of boundaries are oriented at about 40–50° with respect to the compression axis. Such a grain boundary configuration would promote grain boundary sliding at slow strain rates. The microstructure would have resulted due to quick DRX in the initial stages of plastic deformation as suggested by Wu and Liu [17] and followed by grain boundary sliding on continued deformation which may result in wedge cracking.

**Figure 5.** Processing map obtained at a strain of 0.4 for AZ31 magnesium alloy extruded at 300 °C.

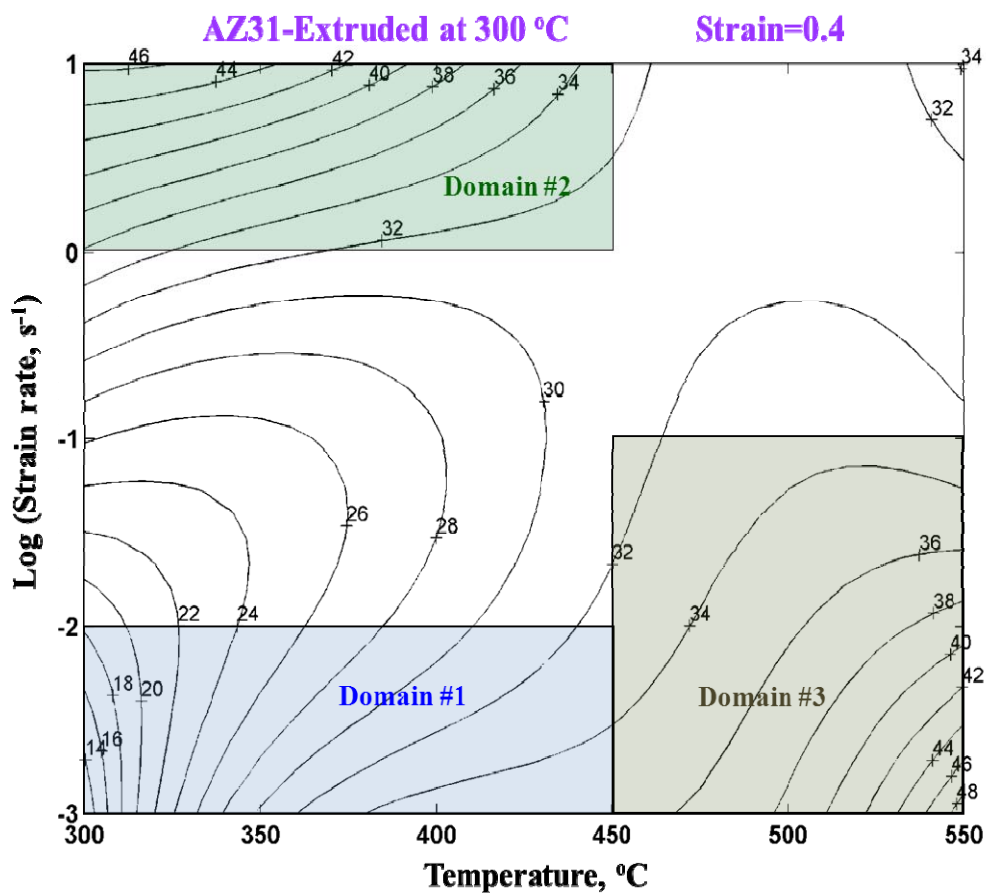
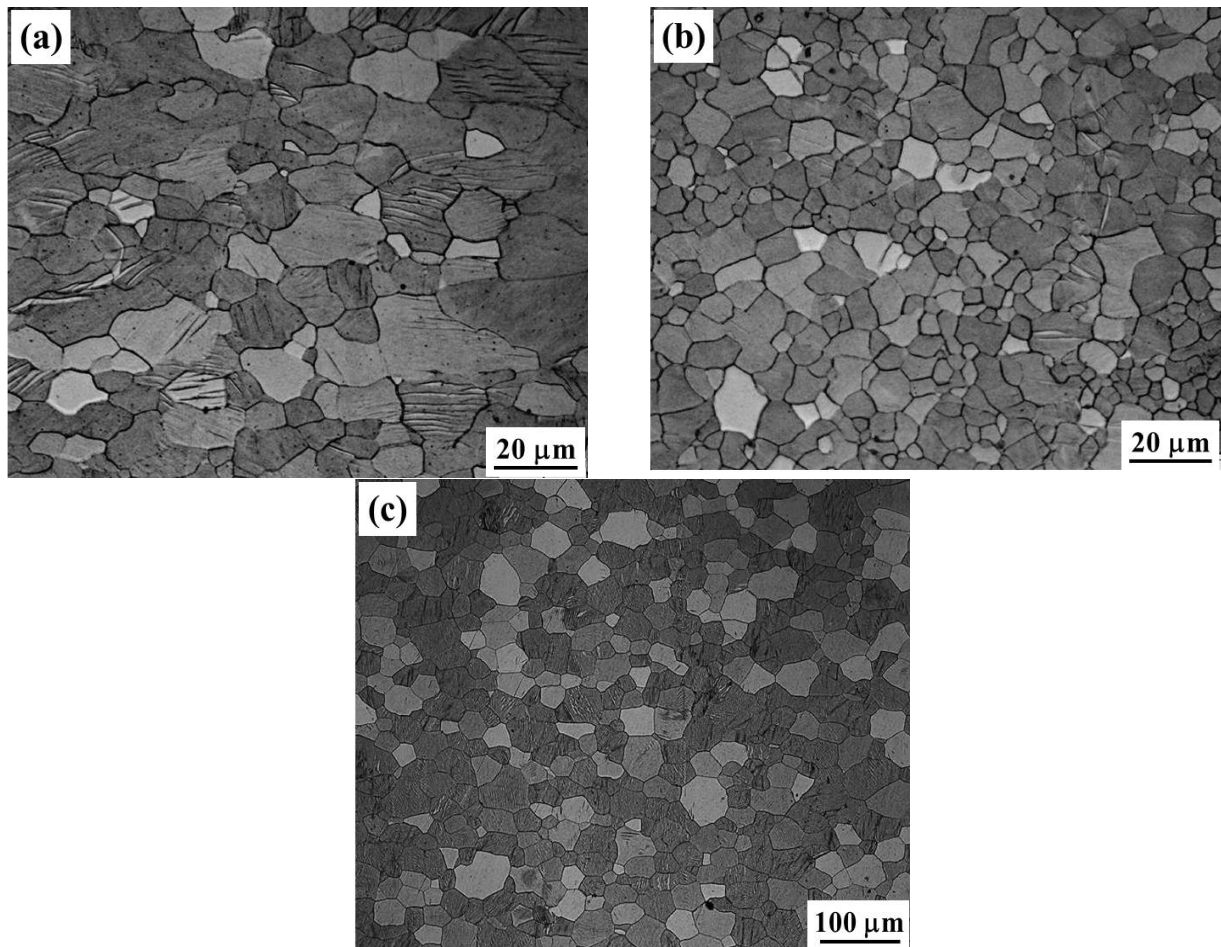


**Figure 6.** Microstructures of AZ31 alloy extruded at 300 °C and compressed at: (a) 400°C/0.001 s<sup>-1</sup> (DRX Domain #1); (b) 300 °C/10 s<sup>-1</sup> (DRX Domain #2); and (c) 550°C/0.001 s<sup>-1</sup> (DRX Domain #3).

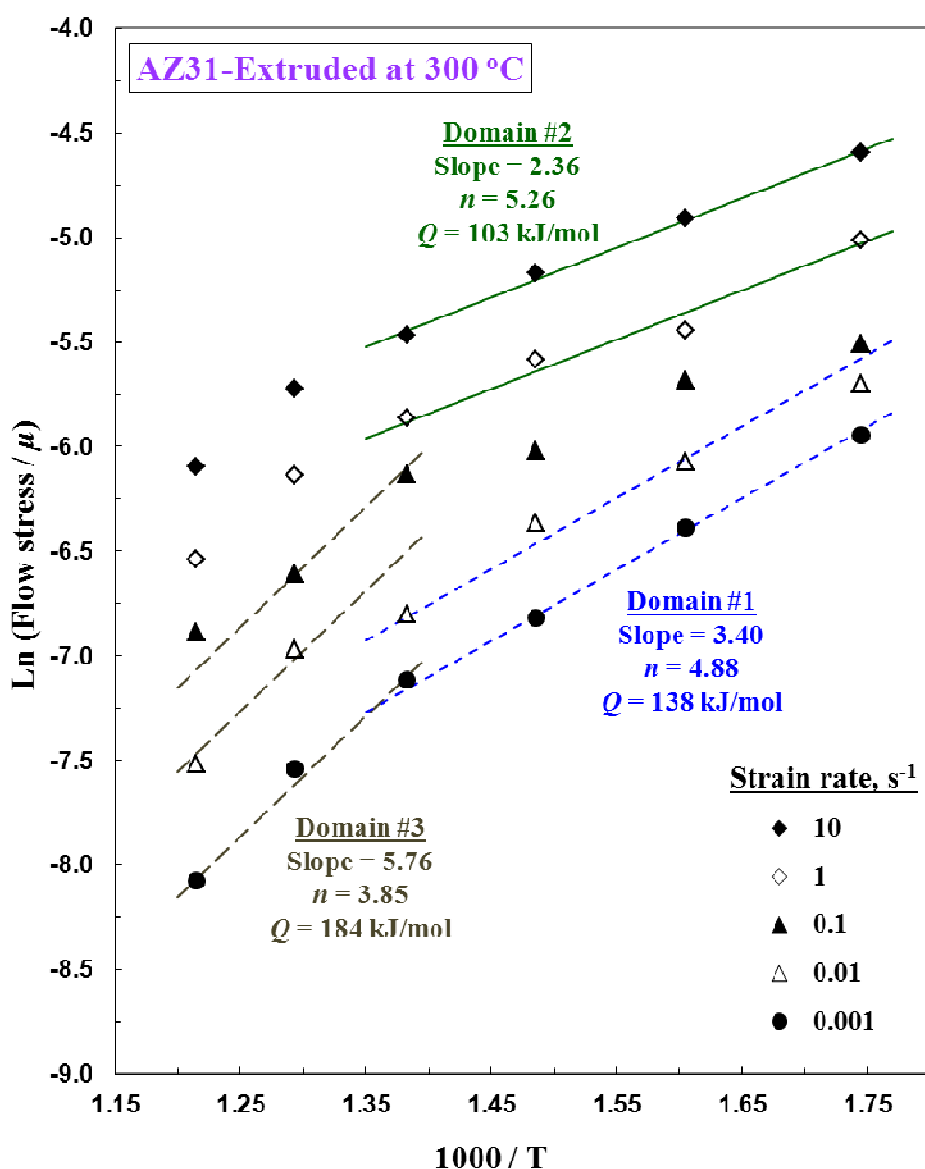


The flow stress data obtained under the conditions corresponding to the above domains are analyzed using the kinetic rate equation, Equation (1), and the activation parameters for DRX are estimated. The Arrhenius plot showing the variation of  $\ln(\sigma/\dot{\mu})$  vs.  $(1/T)$  is shown in Figure 7 which has yielded apparent activation energy values of 138, 103 and 184 kJ/mole in domains #1, #2 and #3, respectively. The results on the domain characteristics and kinetic parameters are summarized in Table 1. These values are close to those obtained on cast-homogenized material with near-random texture and the basic mechanisms controlling hot deformation are apparently unaffected by the texture in the rod extruded at 300 °C.

The effect of rod texture Figure 2(a) with  $\langle 10\bar{1}0 \rangle$  parallel to the extrusion direction on the activation of slip systems when compressed along the extrusion direction may be qualitatively discussed in terms of their relative orientations. The ideal orientation for slip is when the slip plane and slip direction are at 45° with respect to the compression axis since the resolved shear stress will be maximum. For specimens compressed parallel to ED, the  $\{0002\}$  planes are oriented parallel to the compression axis and this reduces the basal slip considerably. According to the standard projection for Mg [47], the  $\{10\bar{1}0\}$  planes are either perpendicular or at 60° with respect to the compression axis, the former orientation reduces prismatic slip but the latter helps since two sets of planes are at this

orientation. The first order pyramidal slip planes  $\{10\bar{1}1\}$  are oriented either at about  $28^\circ$  or at  $46^\circ$  with respect to the compression axis, the latter orientation being highly favorable. The other first order pyramidal plane  $\{10\bar{1}2\}$  will be at  $46^\circ$  or  $60^\circ$  from the compression axis, the former being highly favorable for slip. In all the above cases, the slip direction  $\langle 11\bar{2}0 \rangle$  is oriented either at  $30^\circ$  or  $90^\circ$  from the compression axis, the former one contributing to slip. The second order pyramidal slip planes  $\{11\bar{2}2\}$  are oriented either at  $44^\circ$  or  $90^\circ$  from the compression axis, the former orientation being highly favorable for slip. The slip direction  $\langle 11\bar{2}3 \rangle$  is at about  $50^\circ$  from the compression axis and hence is close to the favorable orientation. In summary, the stronger the fiber  $\langle 10\bar{1}0 \rangle$  texture, the lesser will be basal slip, better will be prismatic slip and higher will be the role of pyramidal slip in the hot deformation. The reduction in basal slip due to texture is probably compensated by increased occurrence of prismatic slip so that no significant changes occur in domains #1 and #2 and domain #3 is better developed since pyramidal slip is enhanced by this texture.

**Figure 7.** Arrhenius plot for calculating apparent activation energy in the three domains of processing map for AZ31 magnesium alloy extruded at  $300^\circ\text{C}$ .

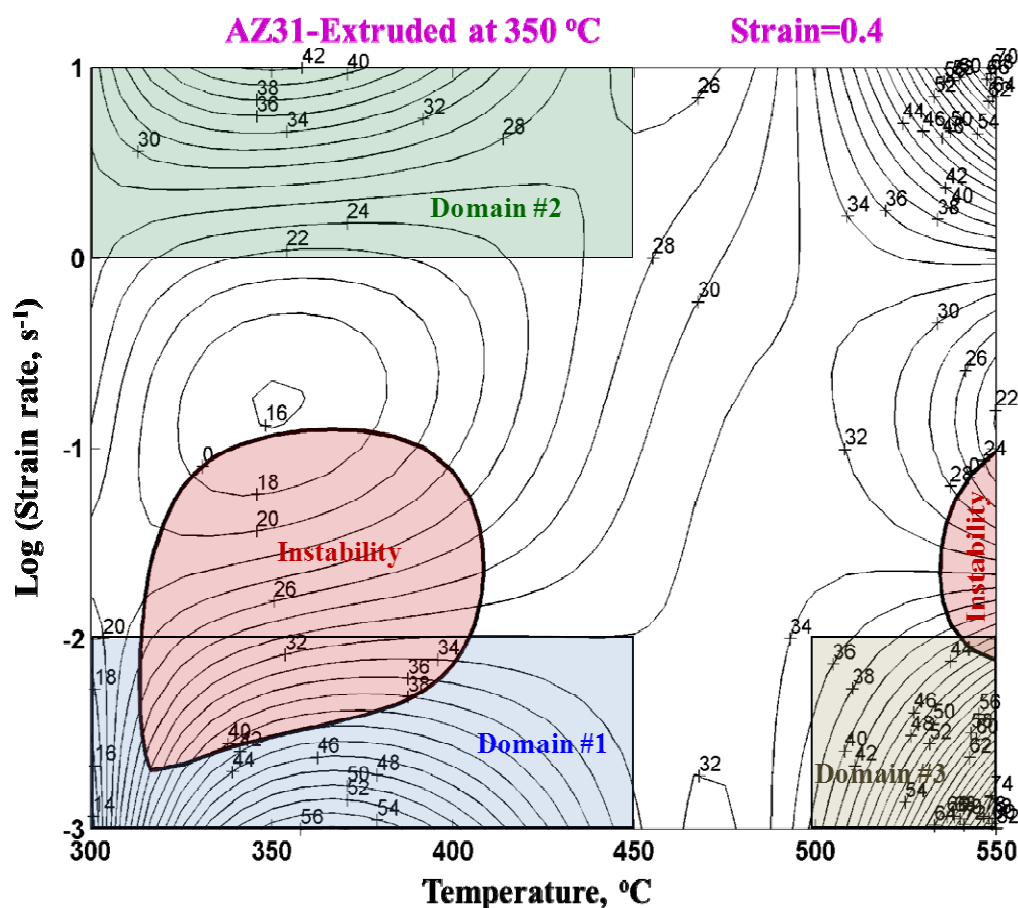


### 3.4. Hot Compression of AZ31 Extruded at 350 °C

The processing map obtained at a strain of 0.4 is shown in Figure 8, which exhibits three domains as described below:

- (i) Domain #1 occurs in the temperature range 300–450 °C and strain rate range 0.001–0.01 s<sup>-1</sup> and has a peak efficiency of about 56% at 375 °C and 0.001 s<sup>-1</sup>.
- (ii) Domain #2 occurs in the temperature range 300–450 °C and strain rate range 1–10 s<sup>-1</sup> and has a peak efficiency of about 42% at 350 °C and 10 s<sup>-1</sup>.
- (iii) Domain #3 occurs in the temperature range 500–550 °C and strain rate range 0.001–0.01 s<sup>-1</sup> and has a peak efficiency of about 82% at 550 °C and 0.001 s<sup>-1</sup>.

**Figure 8.** Processing map obtained at a strain of 0.4 for AZ31 magnesium alloy extruded at 350 °C.

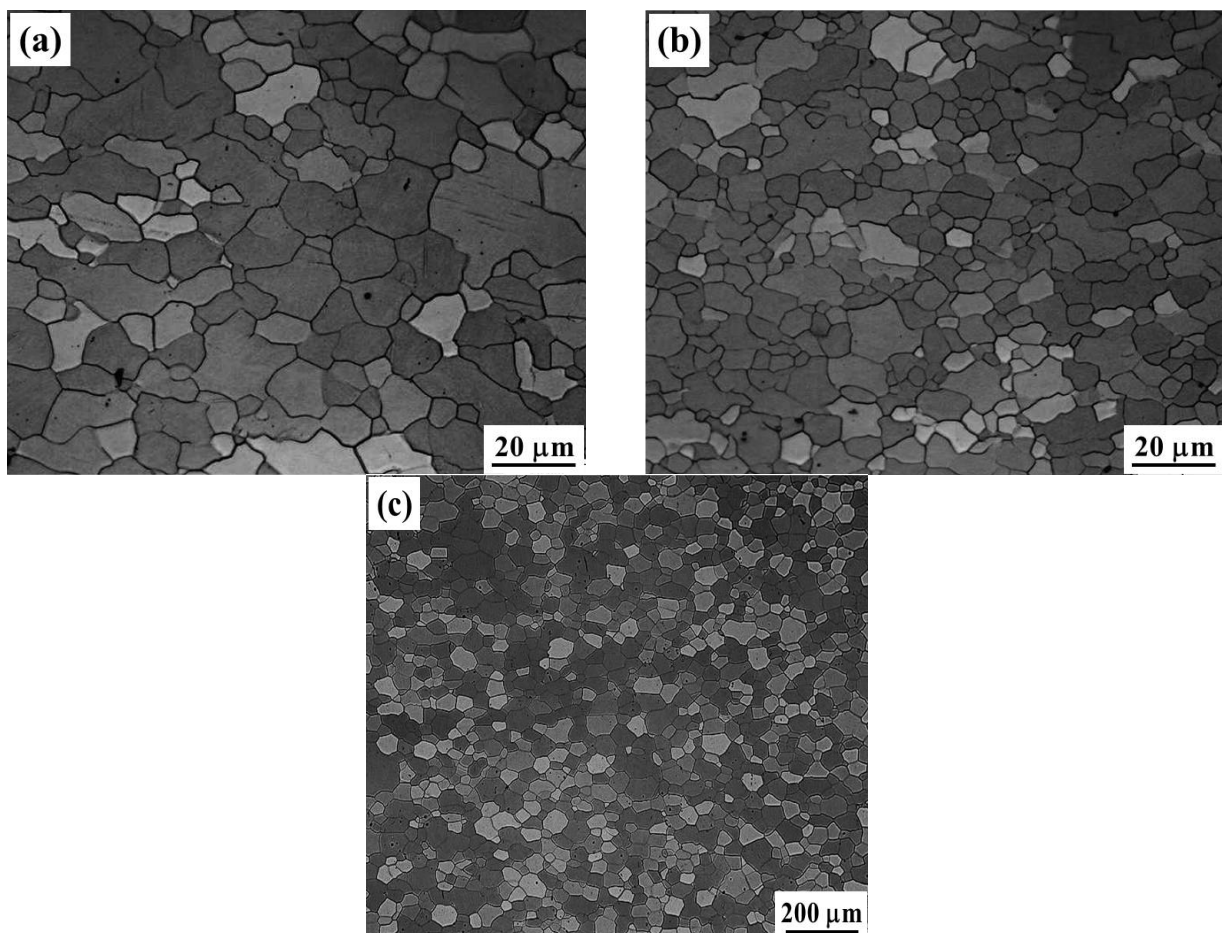


The domains are very similar to those seen in the maps for the cast-homogenized (Figure 3) and the rod extruded at 300 °C (Figure 5), but are well developed with a higher peak efficiency, particularly domains #1 and #3. The domain at high temperatures and high strain rates (right-hand top corner of the map) represents intercrystalline cracking. The flow instabilities are also marginal in terms of their effect on the microstructure. These two are not considered in this discussion.

Referring to domain #1 above, the microstructure of a specimen deformed under conditions near the peak efficiency (350 °C and 0.001 s<sup>-1</sup>) is shown in Figure 9a which represents typical DRX microstructure with many curved boundaries that indicates the occurrence of DRX process. The microstructure of specimen deformed at 350 °C/10 s<sup>-1</sup> (domain #2) is shown in Figure 9b which also

has similar features as in domain #1 and also represents DRX. In domain #3, the efficiency of power dissipation is considerably high which is usually observed in the case of superplastic deformation. The microstructure obtained on a specimen deformed at 550 °C and 0.001 s<sup>-1</sup> Figure 9c exhibits a well-defined grain structure with “diamond” configuration where many of the boundaries are oriented at 40–50° with respect to the compression axis. This grain boundary geometry promotes grain boundary sliding which results in superplasticity or wedge cracking. DRX probably occurs in the early stages of deformation as suggested by Wu and Liu [17] and forms the diamond configuration at larger strains.

**Figure 9.** Microstructures of AZ31 alloy extruded at 350 °C and compressed at: (a) 350 °C/0.001 s<sup>-1</sup> (DRX Domain #1); (b) 350 °C/10 s<sup>-1</sup> (DRX Domain #2); and (c) 550 °C/0.001 s<sup>-1</sup> (DRX Domain #3).

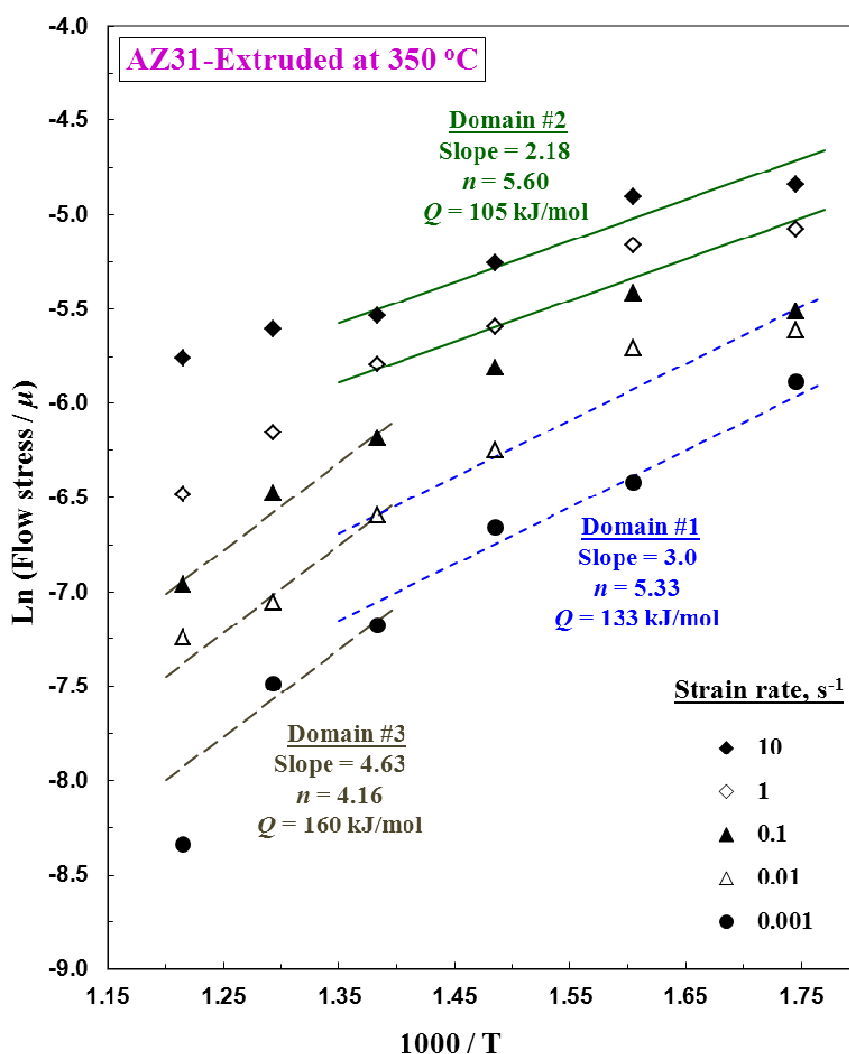


The kinetic analysis involving the evaluation of apparent activation energy from the data within the three domains is shown in Figure 10 in the form of  $\ln(\sigma/\mu)$  vs.  $(1/T)$  plots. Values of apparent activation energy of 133, 105 and 160 kJ/mol have been estimated for domains #1, #2 and #3 respectively which are again similar to those evaluated in the case of cast-homogenized and rod extruded at 300 °C, although slightly lower. The rate controlling mechanisms in domains #1, #2 and #3 are lattice self-diffusion, grain boundary self-diffusion and cross-slip as discussed before. The results on the domain characteristics and kinetic parameters are summarized in Table 1.

The intensity of  $\langle 10\bar{1}0 \rangle$  texture in the rod extruded at 350 °C is highest of all the extruded conditions and as discussed in the previous section, this reduces the participation of basal slip and

increases the contribution of prismatic slip in domains #1 and #2. Because of increased prismatic slip, these two DRX domains become more “efficient” and well defined. The domains become well defined since the recovery mechanism is the same (climb) for both basal and prismatic slip systems. The enhanced occurrence of pyramidal slip caused by this texture causes DRX early in deformation and forms grain boundary geometry in a “diamond” configuration promoting grain boundary sliding which may result in wedge cracking. Thus this intense  $\langle 10\bar{1}0 \rangle$  texture forms well defined domains of workability, increases the efficiency of power dissipation in all the domains and enhances overall workability in all the domains.

**Figure 10.** Arrhenius plot for calculating apparent activation energy in the three domains of processing map for AZ31 magnesium alloy extruded at 350 °C.



### 3.5. Hot Compression of AZ31 Extruded at 450 °C

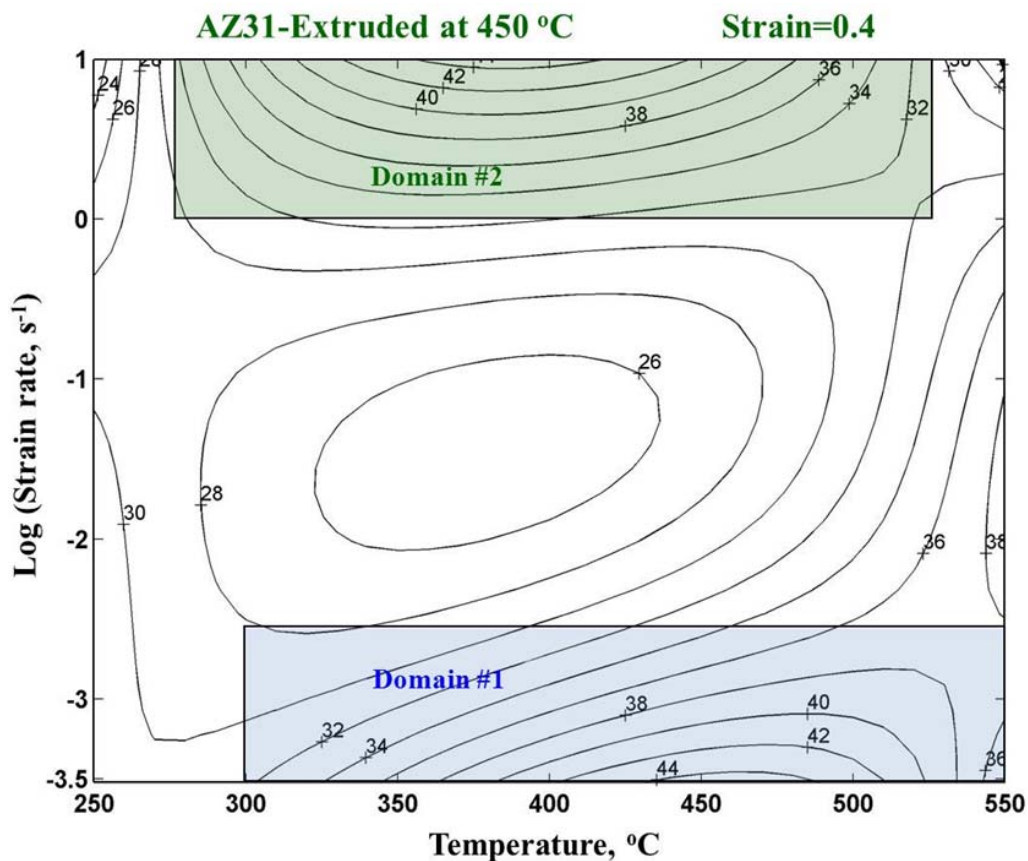
The hot working characteristics of AZ31 rod extruded at 450 °C have been characterized in detail in an earlier publication [48]. The processing map obtained at a strain of 0.4 is shown in Figure 11, which exhibits two domains, one at lower strain rates and the other at higher strain rates, as described below:

- (i) Domain #1 occurs in the temperature range 300–550 °C and strain rate range 0.0003–0.003 s<sup>-1</sup>

with a peak efficiency of about 44% located at 475 °C/0.0003 s<sup>-1</sup>.

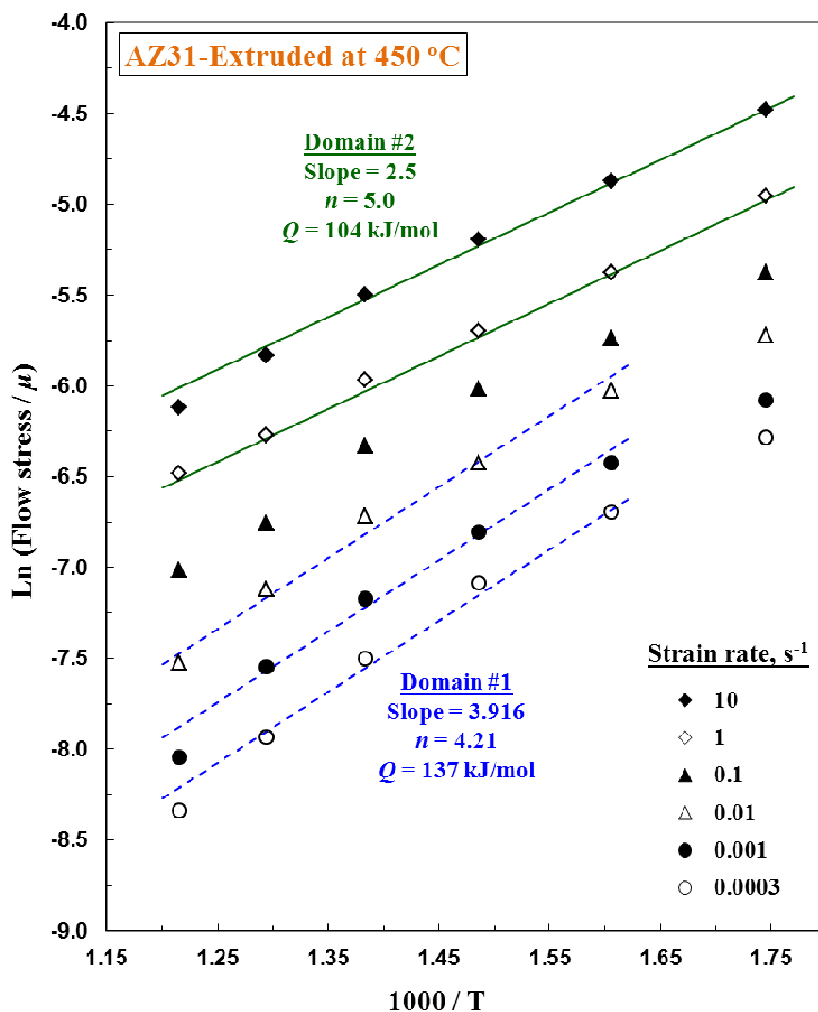
- (ii) Domain #2 occurs in the temperature range 275–525 °C and strain rate range 1–10 s<sup>-1</sup> with a peak efficiency of about 44% located at 400 °C/10 s<sup>-1</sup>.

**Figure 11.** Processing map obtained at a strain of 0.4 for AZ31 magnesium alloy extruded at 450 °C.



The map did not exhibit any regime of flow instability as defined by the criterion given by Equation (3). Detailed microstructural analysis in the domains as well as in the change-over region has already been presented in the earlier publication [48]. Both the domains exhibit dynamically recrystallized grain structures with some curved boundaries. The activation parameters have been evaluated using the kinetic rate equation (Equation 1). The Arrhenius plot showing the variation of  $\ln(\sigma/\dot{\mu})$  vs.  $(1/T)$  for the data corresponding to the two domains, is shown in Figure 12 and the values of apparent activation energy estimated are 137 and 104 kJ/mol for domain #1 and domain #2 respectively. The results on the domain characteristics and kinetic parameters are summarized in Table 1. The apparent activation energy in domain #1 (137 kJ/mol) is nearer that for lattice self-diffusion in magnesium (135 kJ/mol) [46], while that obtained in domain #2 (104 kJ/mol) is near that for grain boundary self-diffusion (92 kJ/mol) [46]. These two domains are similar to domains #1 and #2 of the maps for cast-homogenized material (Figure 3) and rods extruded at 300 °C (Figure 5) and 350 °C (Figure 8), except that the domains moved to higher temperatures covering nearly the entire temperature range. Domain #3 is absent in the map of the rod extruded at 450 °C (Figure 11).

**Figure 12.** Arrhenius plot for calculating apparent activation energy in the two domains of processing map for AZ31 magnesium alloy extruded at 450 °C.



From Figure 2, it is seen that the intensity of  $\langle 10\bar{1}0 \rangle$  texture has decreased to 2.5 times random from a maximum value of 3.75 times random in the rod extruded at 350 °C. The  $\langle 10\bar{1}0 \rangle$  pole also rotates away from the extrusion axis causing changes in the orientations of basal, prismatic as well as pyramidal slip planes and directions. The reduced  $\langle 10\bar{1}0 \rangle$  intensity and the rotation does not affect the basal slip much but makes the occurrence prismatic slip more difficult and that of pyramidal slip even more difficult. In view of this, domain #3 is absent due to the curtailment of pyramidal slip and higher temperatures are required for prismatic slip to occur in domains #1 and #2. Thus, the texture obtained in the rod extruded at 450 °C is less favorable for workability than the ones extruded at 300 °C and 350 °C.

#### 4. Conclusions

On the basis of kinetic analysis and processing maps for hot deformation obtained on AZ31 magnesium alloy extruded at different temperatures, the following conclusions are drawn:

- (i) The AZ31 alloy rods exhibited  $\langle 10\bar{1}0 \rangle$  fiber texture, the intensity of which increased when extruded at 300 °C and 350 °C but the texture was weakened and  $\langle 10\bar{1}0 \rangle$  pole rotated away from the extrusion direction when extruded at 450 °C.
- (ii) The processing maps for AZ31 with near-random texture (cast-homogenized), and rods extruded at 300 °C as well as 350 °C exhibited three DRX domains in the general temperature strain rate ranges of: (1) 300–450 °C and 0.001–0.01 s<sup>-1</sup>, (2) 300–450 °C and 1–10 s<sup>-1</sup>, and (3) 450–550 °C and 0.001–0.1 s<sup>-1</sup>, while the material extruded at 450 °C exhibited only domains #1 and #2 at higher temperatures.
- (iii) In domains #1 and #2, prismatic slip is the dominant process and DRX is controlled by lattice self-diffusion and grain boundary self-diffusion, respectively, while in domain #3, pyramidal slip occurs extensively and DRX is controlled by cross-slip on pyramidal systems.
- (iv) Intense  $\langle 10\bar{1}0 \rangle$  fiber texture, as in the rod extruded at 350 °C, will enhance the occurrence of prismatic slip in domains #1 and #2 and promotes pyramidal slip at temperatures >450 °C (domain #3).
- (v) When the texture is weakened and rotated as in the rod extruded at 450 °C, domains #1 and #2 move to higher temperatures due to higher difficulty for the occurrence of prismatic slip, while domain #3 does not occur due to the curtailment of pyramidal slip.

## Acknowledgments

The work presented in this paper has been supported by strategic research grants (#7008098 and #7002704) from City University of Hong Kong and General Research Fund (#114811) from the Research Grants Council of the University Grants Council, Hong Kong Special Administrative Region. The authors would like to thank to J. Bohlen and T. Abu Leil of Helmholtz Zentrum Geesthacht, Germany, for their help in part of the texture work, and K. Suresh, City University of Hong Kong, for his assistance in the preparation of the manuscript.

## Conflict of Interest

The authors declare no conflict of interest.

## References

1. Kainer, K.U.; Dieringa, H.; Dietzel, W.; Hort, N.; Blawert, C. The use of magnesium alloys: Past, present and future. In *Magnesium Technology in the Global Age*, Proceedings of the International Symposium on Magnesium Technology in the Global Age, Montreal, PQ, Canada, 1–4 October 2006; Pekguleryuz, M.O., Mackenzie, L.W.F., Eds.; Canadian Institute of Mining, Metallurgy and Petroleum: Montreal, Quebec, Canada, 2006; pp. 3–19.
2. Beer, A.G.; Barnett, M.R. Influence of initial microstructure on the hot working flow stress of Mg-3Al-1Zn. *Mater. Sci. Eng. A* **2006**, *423*, 292–299.
3. Yi, S.B.; Zaefferer, S.; Brokmeier, H.G. Mechanical behaviour and microstructural evolution of magnesium alloy AZ31 in tension at different temperatures. *Mater. Sci. Eng. A* **2006**, *424*, 275–281.

4. Tian, S.; Wang, L.; Sohn, K.Y.; Kim, K.H.; Xu, Y.; Hu, Z. Microstructure evolution and deformation features of AZ31 Mg-alloy during creep. *Mater. Sci. Eng. A* **2006**, *415*, 309–316.
5. Murai, T.; Matsuoka, S.I.; Miyamoto, S.; Oki, Y. Effects of extrusion conditions on microstructure and mechanical properties of AZ31B magnesium alloy extrusions. *J. Mater. Process. Tech.* **2003**, *141*, 207–212.
6. Barnett, M.R.; Keshavarz, Z.; Beer, A.G.; Atwell, D. Influence of grain size on the compressive deformation of wrought Mg-3Al-1Zn. *Acta Mater.* **2004**, *52*, 5093–5103.
7. Huang, C.C.; Huang, J.C.; Lin, Y.K.; Hwang, Y.M. Basal-texture induced low formability during room temperature hydroforming of fine-grained AZ31 Mg tubes. *Mater. Trans.* **2004**, *45*, 3142–3149.
8. Chino, Y.; Sassa, K.; Kamiya, A.; Mabuchi, M. Enhanced formability at elevated temperature of a cross-rolled magnesium alloy sheet. *Mater. Sci. Eng. A* **2006**, *441*, 349–356.
9. Uematsu, Y.; Tokaji, K.; Kamakura, M.; Uchida, K.; Shibata, H.; Bekku, N. Effect of extrusion conditions on grain refinement and fatigue behaviour in magnesium alloys. *Mater. Sci. Eng. A* **2006**, *434*, 131–140.
10. Watanabe, H.; Takara, A.; Somekawa, H.; Mukai, T.; Higashi, K. Effect of texture on tensile properties at elevated temperatures in an AZ31 magnesium alloy. *Scripta Mater.* **2005**, *52*, 449–454.
11. Helis, L.; Okayasu, K.; Fukutomi, H. Microstructure evolution and texture development during high-temperature uniaxial compression of magnesium alloy AZ31. *Mater. Sci. Eng. A* **2006**, *430*, 98–103.
12. Muller, K.B. Direct and Indirect Extrusion of AZ31. In *Magnesium Technology 2002*, Proceedings of the Symposium jointly sponsored by the Magnesium Committee of the Light Metals Division (LMD) of TMS (The Minerals, Metals & Materials) with the International Magnesium Association, Seattle, WA, USA, 17–21 February 2002; Kaplan, H.J., Ed.; TMS: Warrendale, PA, USA, 2002; pp. 187–192.
13. Li, L.; Zhou, J.; Duszczek, J. Determination of a constitutive relationship for AZ31B magnesium alloy and validation through comparison between simulated and real extrusion. *J. Mater. Process. Tech.* **2006**, *172*, 372–380.
14. Lapovok, R.Y.; Barnett, M.R.; Davies, C.H.J. Construction of extrusion limit diagram for AZ31 magnesium alloy by FE simulation. *J. Mater. Process. Tech.* **2004**, *146*, 408–414.
15. Letzig, D.; Swiostek, J.; Bohlen, J.; Beaven, P.A. Extrusion of AZ-Series Magnesium alloys. In *Magnesium Technology in the Global Age*, Proceedings of the International Symposium on Magnesium Technology in the Global Age, Montreal, PQ, Canada, 1–4 October 2006; Pegguleryuz, M.O., Mackenzie, L.W.F., Eds.; Canadian Institute of Mining, Metallurgy and Petroleum: Montreal, Quebec, Canada, 2006; pp. 569–580.
16. Prasad, Y.V.R.K.; Rao, K.P. Effect of crystallographic texture on the kinetics of hot deformation of rolled Mg-3Al-1Zn alloy plate. *Mater. Sci. Eng. A* **2006**, *432*, 170–177.
17. Wu, X.; Liu, Y. Superplasticity of coarse-grained magnesium alloy. *Scripta Mater.* **2002**, *46*, 269–274.
18. Tan, J.C.; Tan, M.J. Superplasticity and grain boundary sliding characteristics in two stage deformation of Mg-3Al-1Zn alloy sheet. *Mater. Sci. Eng. A* **2003**, *339*, 81–89.
19. Prasad, Y.V.R.K.; Rao, K.P. Hot workability, microstructural control and rate-controlling mechanisms in cast-homogenized AZ31 magnesium alloy. *Adv. Eng. Mater.* **2009**, *11*, 182–188.

20. Jonas, J.J.; Sellars, C.M.; Tegart, W.J.M. Strength and structure under hot-working conditions. *Metall. Rev.* **1969**, *14*, 1–24.
21. McQueen, H.J. Hot Workability of Mg Alloys-Insights from Al Alloys. In *Magnesium Technology in the Global Age*, Proceedings of the International Symposium on Magnesium Technology in the Global Age, Montreal, PQ, Canada, 1–4 October 2006; Pekguleryuz, M.O., Mackenzie, L.W.F., Eds.; Canadian Institute of Mining, Metallurgy and Petroleum: Montreal, QC, Canada, 2006; pp. 399–420.
22. Spigarelli, S.; Mehtedi, M.El.; Evangelista, E.; Kaneko, J. High temperature plastic deformation of a heat-treated AZ31 magnesium alloy. *Metall. Sci. Tech.* **2005**, *23*, 11–17.
23. McQueen, H.J.; Myshleyaev, M.; Mwembala, A.; Konopleva, E.V. Hot Working Characteristics of Mg-2.8Al-0.9Zn. In *Magnesium Alloys and Their Applications*; Proceedings of the International Conference and Exhibition Magnesium Alloys and their Applications, Wolfsburg, Germany, 28–30 April 1998; Mordike, B.L., Kainer, K.U., Eds.; Werkstoff Info-Gesellschaft: Frankfurt, Germany, 1998; pp. 201–208.
24. Liu, W.J.; Kao, V.; Essadiqi, E.; Elwazri, A.; Yue, S.; Verma, R. Dynamic recrystallization of AZ31 magnesium alloy during torsion deformation at elevated temperatures. In *Magnesium Technology 2004*, Proceedings of the Symposium held during the 2004 TMS Annual Meeting, Charlotte, NC, USA, 14–18 March 2004; Luo, A.A., Ed.; TMS: Warrendale, PA, USA, 2004; pp. 73–78.
25. Chabbi, L.; Lehnert, W. Hot and cold forming behaviour of Mg-materials. In *Magnesium Alloys and Their Applications*, Proceedings of the International Conference and Exhibition Magnesium Alloys and their Applications, Wolfsburg, Germany, 28–30 April 1998; Mordike, B.L., Kainer, K.U., Eds.; Werkstoff Info-Gesellschaft: Frankfurt, Germany, 1998; pp. 313–317.
26. Beer, A.G.; Barnett, M.R. The hot working flow stress and microstructure in magnesium AZ31. In *Magnesium Technology 2002*, Proceedings of the Symposium jointly sponsored by the Magnesium Committee of the Light Metals Division (LMD) of TMS (The Minerals, Metals & Materials) with the International Magnesium Association, Seattle, WA, USA, 17–21 February 2002; Kaplan, H.J., Ed.; TMS: Warrendale, PA, USA, 2002; pp. 193–198.
27. Prasad, Y.V.R.K.; Seshacharyulu, T. Modeling of hot deformation for microstructural control. *Int. Mater. Rev.* **1998**, *43*, 243–258.
28. Prasad, Y.V.R.K.; Sasidhara, S. *Hot Working Guide: A Compendium of Processing Maps*; ASM International: Novelt, OH, USA, 1997.
29. Prasad, Y.V.R.K. Processing maps: A status report. *J. Mater. Eng. Perform.* **2003**, *12*, 638–645.
30. Ziegler, H. In *Progress in Solid Mechanics*; Sneddon, I.N., Hill, R., Eds.; John Wiley: New York, NY, USA, 1965; pp. 91–193.
31. Prigogine, I. Time, structure, and fluctuations. *Science* **1978**, *201*, 777–785.
32. Wang, Y.; Zhang, Y.; Zeng, X.; Ding, W. Characterization of dynamic recrystallization in as-homogenized Mg-Zn-Y-Zr alloy using processing map. *J. Mater. Sci.* **2006**, *41*, 3603–3608.
33. Dzwonczyk, J.; Prasad, Y.V.R.K.; Hort, N.; Kainer, K.U. Enhancement of workability in AZ31 alloy-processing maps: Part I, cast material. *Adv. Eng. Mater.* **2006**, *8*, 966–973.
34. Wang, C.Y.; Wang, X.J.; Chang, H.; Wu, K.; Zheng, M.Y. Processing maps for hot working of ZK60 magnesium alloy. *Mater. Sci. Eng. A* **2007**, *464*, 52–58.

35. Slooff, F.A.; Dwonczyk, J.S.; Zhou, J.; Duszczynk, J.; Katgerman, L. Hot workability analysis of extruded AZ magnesium alloys with processing maps. *Mater. Sci. Eng. A* **2010**, *527*, 735–744.
36. Chen, Z.; Li, Z.; Yu, C. Hot deformation behavior of an extruded Mg-Li-Zn-RE alloy. *Mater. Sci. Eng. A* **2011**, *528*, 961–966.
37. Liu, R.; Cao, W.; Fan, T.; Zhang, C.; Zhang, D. Development of processing maps for 3 vol.% TiCp/AZ91D composites material. *Mater. Sci. Eng. A* **2010**, *527*, 4687–4693.
38. Li, L.; Zhang, X. Hot compression deformation behavior and processing parameters of a cast Mg-Gd-Y-Zr alloy. *Mater. Sci. Eng. A* **2011**, *528*, 1396–1401.
39. Li, H.Z.; Wang, H.J.; Li, Z.; Liu, C.M.; Liu, H.T. Flow behavior and processing map of as-cast Mg-10Gd-4.8Y-2Zn-0.6Zr alloy. *Mater. Sci. Eng. A* **2010**, *528*, 154–160.
40. Rao, K.P.; Prasad, Y.K.; Dharmendra, C.; Hort, N.; Kainer, K.U. Compressive strength and hot deformation behavior of TX32 magnesium alloy with 0.4% Al and 0.4% Si additions. *Mater. Sci. Eng. A* **2011**, *528*, 6964–6970.
41. Rao, K.P.; Prasad, Y.K.; Hort, N.; Kainer, K.U. High temperature deformation mechanisms and processing map for hot working of cast-homogenized Mg-3Sn-2Ca alloy. *Mater. Sci. Forum* **2010**, *638–642*, 3616–3621.
42. Prasad, Y.V.R.K.; Rao, K.P. Processing maps and rate controlling mechanisms of hot deformation of electrolytic tough pitch copper in the temperature range 300–950 °C. *Mater. Sci. Eng. A* **2005**, *391*, 141–150.
43. Brokmeier, H.G.; Gunther, A.; Yi, S.B.; Ye, W.; Lippmann, T.; Garbe, U. Investigation of local textures in extruded magnesium by synchrotron radiation. *Adv. X Ray Anal.* **2003**, *46*, 151–156.
44. Sastry, D.H.; Prasad, Y.V.R.K.; Vasu, K.I. On the stacking fault energies of some close-packed hexagonal metals. *Scripta Metall.* **1969**, *3*, 927–929.
45. Morris, J.R.; Scharff, J.; Ho, K.M.; Turner, D.E.; Ye, Y.Y.; Yoo, M.H. Prediction of a {1122} hcp stacking fault using a modified generalized stacking-fault calculation. *Philos. Mag. A* **1997**, *76*, 1065–1077.
46. Frost, H.J.; Ashby, M.F. *Deformation Mechanism Maps*; Pergamon Press: Oxford, UK, 1982.
47. Taylor, A. *X-ray Metallography*; John Wiley & Sons Inc: New York, NY, USA, London, UK, 1961; p. 44, 572.
48. Prasad, Y.V.R.K.; Rao, K.P. Hot deformation mechanisms and microstructural control in high-temperature extruded AZ31 magnesium alloy. *Adv. Eng. Mater.* **2007**, *9*, 558–565.